JACS
JOURNAL OF THE AMERICAN CHEMICAL SOCIETY
Communication
pubs.acs.org/JACS

Effective Ligand Passivation of Cu_2O Nanoparticles through Solid-State Treatment with Mercaptopropionic Acid

Hamed Azimi,*[,†] Susanne Kuhri,[‡] Andres Osvet,[†] Gebhard Matt,[†] Laraib S. Khanzada,[†] Mario Lemmer,[†] Norman A. Luechinger,[§] Mats I. Larsson,[∥] Eitan Zeira,[∥] Dirk M. Guldi,[‡] and Christoph J. Brabec[†,⊥]

[†]Institute of Materials for Electronics and Energy Technology (I-MEET), Department of Materials Science and Engineering, Friedrich-Alexander University Erlangen-Nuremberg, Martensstrasse 7, 91058 Erlangen, Germany

[‡]Department of Chemistry and Pharmacy and Interdisciplinary Center for Molecular Materials, Friedrich-Alexander-University Erlangen-Nuremberg, 91058 Erlangen, Germany

[§]Nanograde Llc., Laubisruetistrasse 50, 8712 Staefa, Switzerland

[∥]OneSun Inc., P.O. Box 1399, Sausalito, California 94966, United States

[⊥]Bavarian Center for Applied Energy Research (ZAE Bayern), Haberstr. 2a, 91058 Erlangen, Germany

Supporting Information

ABSTRACT: In colloidal nanoparticle (NPs) devices, trap state densities at their surface exert a profound impact on the rate of charge carrier recombination and, consequently, on the deterioration of the device performance. Here, we report on the successful application of a ligand exchange strategy to effectively passivate the surface of cuprite (Cu_2O) NPs. Cu_2O NPs were prepared by means of a novel synthetic route based on flame spray pyrolysis. FTIR, XRD, XPS, and HRTEM measurements corroborate the formation of cubic cuprite Cu_2O nanocrystals, excluding the possible presence of undesired CuO or Cu phases. Most importantly, steady-state emission and transient absorption assays document that surface passivation results in substantial changes in the intensity of emissive excitonic states—centered at copper and oxygen vacancies—and in the lifetime of excitons near the band edge. To shed light onto ultrafast processes in Cu_2O nanocrystals additional pump probe experiments on the femtosecond and nanosecond time scales were carried out. Two discernible species were observed: on one hand, an ultrafast component (∼ps) that relates to the excitons; on the other hand, a long-lived component (∼μs) that originates from the defects/trap states.

Metal oxide semiconductors offer a broad range of attractive properties, including chemical stability, nontoxicity, and high abundance of elements.[1,2] Recently, special attention has been paid to preparing and probing colloidal nanoparticles (NPs) of copper oxide in the context of various photonic and photoelectrochemical applications.[3−6] Cuprous oxide (cuprite Cu_2O), which features p-type semiconducting properties and a band gap energy of about 2.1 eV, has emerged as an interesting class of materials for solar energy conversion.[7,8]

In the synthesis of cuprous oxide NPs, one of the grand challenges is the synthesis of high-quality Cu_2O NPs with minimum imperfections and the inclusion portions of impurities or undesired phases. Importantly, the formation of CuO or Cu phases on the surface of Cu_2O NPs may exceed the deleterious impact on the semiconducting properties of cuprous oxide films. In addition, important challenges in colloidal NP devices encompass the presence of an organic capping agent, on one hand, and the existence of various bulk and/or surface trap states, on the other hand. The earlier and the latter are both crucial factors that impact excited state carrier dynamics as well as charge transport in optoelectronic devices.

Disorders, reconstructions, and uncoordinated atoms on the surface evoke the formation of shallow and deep traps in NP devices, which may adversely impact the device performance.[9] A potential solution to overcome the detrimental influence of surface traps implies the ligand passivation of NPs through a simple post-solid-state treatment. Past work has demonstrated that monovalent inorganic ligands bound to cations provide the necessary means to effectively surface passivate NPs.[10] A particularly crucial advantage of this approach is the possibility to remove dangling bonds at the NP surface without the requirements to carry out any high temperature processing steps. To date, this strategy is, however, only applied to a few inorganic NP systems such as PbS, PbSe, CdS, and CdTe NPs.[11,12] Here, we report the preparation of single phase Cu_2O nanocrystals. The dry Cu_2O nanopowder was prepared by flame spray synthesis, whereby the flame was run in nitrogen, that is, under nonoxidizing conditions, to avoid the formation of fully oxidized CuO. Cu_2O NPs were then dispersed in an acetic acid/isopropanol solvent mixture (5 wt %). The resulting mixture was centrifuged, and the supernatant was removed and replaced by dry isopropanol. The Cu_2O sediment was again dispersed with the help of horn sonication and centrifuged. After repeated washing and centrifugation, isopropanol was added in order to adjust the Cu_2O solid concentration to 5 wt %; for further details on the synthesis of Cu_2O NPs, see the Supporting Information (SI). The postsynthetic ligand exchange on thin films is exploited effectively to eliminate surface recombination sites in Cu_2O NPs.

Figure 1a shows X-ray diffraction (XRD) patterns of as-synthesized Cu_2O NPs. The observed diffraction peaks are indexed as (110), (111), (200), and (220) reflections of the

Received: March 11, 2014
Published: May 5, 2014

   dx.doi.org/10.1021/ja502221r | J. Am. Chem. Soc. 2014, 136, 7233−7236

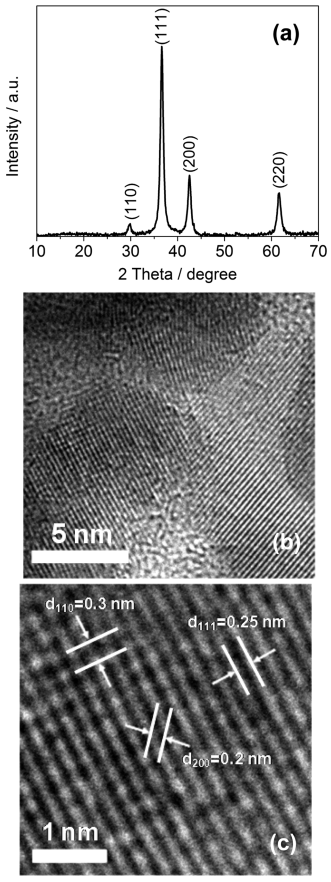

Figure 1. (a) X-ray powder diffraction patterns of as-synthesized Cu_2O NPs. (b) HRTEM image of Cu_2O NPs. (c) Corresponding zoom-in HRTEM image of a single Cu_2O NP whose infringe spacings match those of the Cu_2O cuprite. The lattice spacings for the (110), (111), and (200) planes are 0.3, 0.25, and 0.2 nm, respectively.

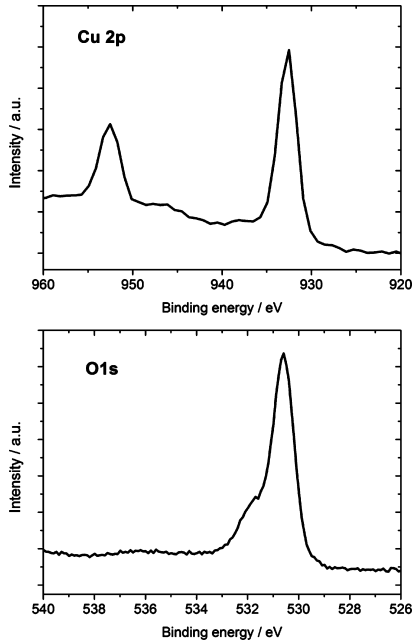

Figure 2. XP high-resolution spectra of Cu_2O NPs displaying the Cu 2p and O 1s regions.

standard cubic cuprite crystal structure with a lattice constant of 4.27 Å (space group $Pn\bar{3}m$ or O_h^4). Similar to bulk cubic Cu_2O (JCPDS No. 05-0667), a stronger intensity of the (200) peak is noted when compared to that of the (220) peak. The phase and purity of Cu_2O NPs is further studied by high-resolution transmission electron microscopy (HRTEM). From the HRTEM images (see Figure 1b, c) the high crystallinity of Cu_2O NPs is appreciated. Moreover, atomic lattice fringes with interplanar spacings of 2, 2.5, and 3 Å are resolved, which match well with the lattice planes of (200), (111), and (110) of cubic Cu_2O, respectively.

To further examine the quality of the Cu_2O NPs and their surface chemical interactions, a surface sensitive technique such as X-ray photoelectron spectroscopy (XPS) was employed. In the XPS spectrum of the copper core level, namely Cu 2p, shown in Figure 2, the main peaks at 932.5 and 952.6 eV correlate with Cu $2p_{3/2}$ and Cu $2p_{1/2}$, respectively, and are assigned to Cu^+, while signals associated with Cu^{2+} or $Cu^{\pm 0}$ are lacking. In the Cu 2p spectrum, Cu^{2+} is identified by the appearance of a main signal at 933.5 eV along with a series of shakeup satellites at higher binding energies.[13] The shakeup satellites are characteristic of materials such as Cu^{2+} having a partially filled d^9 shell configuration in the ground state. The absence of sharp satellite features for Cu_2O is rationalized on the basis of a full d^{10} shell that inhibits screening via charge transfer involving d states. As a matter of fact, screening the core hole is only realized through states involving the broad sp conduction band.[14]

Furthermore, in the O 1s spectrum (Figure 2), the main signal at a binding energy of 530.5 eV is a clear oxygen signature associated with cuprite Cu_2O.[15] The shoulder at a slightly higher binding energy of 531.6 eV is ascribed to, for example, hydroxyl groups and molecular water adsorbed on the Cu_2O NP surface.[16,17] Also, the Cu_2O NPs show an LMM Auger transition at 570 eV, which further corroborates the presence of Cu_2O (see Figure S1). In the Cu LMM spectrum, Cu and Cu_2O relate to peaks at 568 and 570 eV, respectively.

Surface passivation of Cu_2O NPs was achieved using a solid-state treatment by 3-mercaptopropionic acid (MPA). Prior to the layer-by-layer washing with MPA, Fourier transform infrared spectroscopy (FTIR) measurements (Figure S2) reveal a signal at 615 cm^{-1}. The latter is associated with copper−oxygen stretching vibrations in the Cu_2O phase.[18] After MPA treatment, additional IR signals are discernible at 1261, 1388, and 1540 cm^{-1}. The peak at 1540 cm^{-1} is assigned to the stretching vibrations of the carbonyl group, while the signals at 1261 and 1388 cm^{-1} are attributable to C−OH and C−O stretching vibrations, respectively. An interesting observation is the lack of S−H stretching, which implies that the mercapto group and Cu^+ form a complex. In turn, this would leave the polar carboxylic acid group retaining the surface of Cu_2O NPs. XPS measurements were also performed with passivated Cu_2O NPs (see Figure S3), indicating the existence of Cu predominantly in the form of Cu_2O. Sulfur (S) was found primarily as a sulfide and/or mercaptan with, however, low levels of sulfate and/or sulfone. In line with the FTIR data, vide supra, these results suggest the complexation of Cu^+ by mercapto groups. We cannot rule out the presence of a small fraction of Cu as Cu sulfide and/or Cu sulfate.

Photoluminescence (PL) spectroscopy was used to study the impact of MPA treatment on the excitonic states in Cu_2O NPs. From the PL spectra of Cu_2O NPs shown in Figure 3, two distinct emission maxima originating from the relaxed excitons localized near Cu and O vacancies are observed. On one hand, the maximum at around 750 nm is associated with the recombination of bound excitons at charged oxygen vacancies

dx.doi.org/10.1021/ja502221r | J. Am. Chem. Soc. 2014, 136, 7233−7236

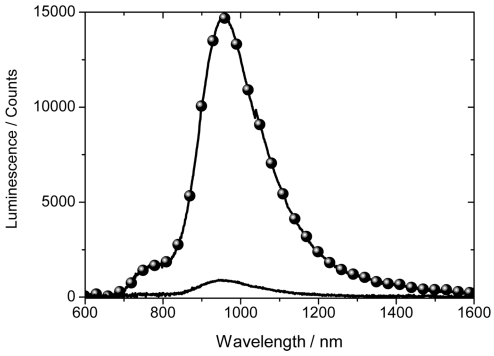

Figure 3. Photoluminescence spectra of Cu_2O NP films before (solid line) and after washing with MPA (solid line with full circles).

(V_O), and on the other hand, the stronger emission maximum at around 960 nm relates to the emission from excitons bound by copper vacancies (V_{Cu}) also known as β-luminescence.[19,20] Large widths of the observed emissions are an indication of strong lattice relaxation within the vicinity of localized excitons.[19] A comparison of emission intensities, that is, 750 vs 960 nm, suggests a higher concentration of V_{Cu} than V_O in Cu_2O NPs. Upon MPA treatment, a substantial increase in the intensity of bound exciton emissions from both V_{Cu} and V_O is seen. The enhanced quantum yield for radiative excitons is explained on the grounds of passivating defects or trap states at the Cu_2O NP surface. These defects and trap states act as recombination centers for charges that dissociate from either Cu or O vacancies. It is noteworthy to emphasize that, in the MPA treated Cu_2O NPs, the increase in PL intensity for V_{Cu} is about twice that for V_O. As copper vacancies are known to be energetically the most favorable p-type defects in Cu_2O,[21] our observation prompts us toward improvement in the p-type conduction properties of MPA modified Cu_2O NPs. Notably, it has been shown that the V_O defects lack transition levels within the gap and, in turn, are incapable of annihilating holes.[21]

To shed light onto the processes following photoexcitation, transient pump probe measurements were performed with femtosecond excitation at 387 nm. First, nonpassivated Cu_2O NPs were probed. Immediately after excitation, an instantaneously formed ground state bleaching is discernible in the 420 to 470 nm range that maximizes at 455 nm, left part of Figure 4. The latter correlates well with the absorption features in terms of band gap seen in the steady state absorption measurements (see Figure S4). Simultaneous with the latter, a broadly absorbing transient is formed, which spans from 470 to 800 nm. It features a maximum at 495 nm and a shoulder at 605 nm and is ascribed to a Cu_2O exciton. Both, that is, the 455 nm minimum and the 500 nm maximum, decay biexponentially. On one hand, a short-lived component of large amplitude is noted within the time window of 20 ps. From a multiwavelength analysis a lifetime of 0.5 ± 0.06 ps is derived for the underlying excitonic state. Implicit is that the presence of defect and/or trap states deactivates the excitonic state rapidly. On the other hand, a long-lived component of small amplitude evolves that is, however, stable beyond the experimental time window of 8 ns. Its two lifetimes, which is in the hundreds of ns and about 2 μs, is only determined in complementary nanosecond pump probe experiments (see Figure S7). Notably, in the long-lived component the minimum

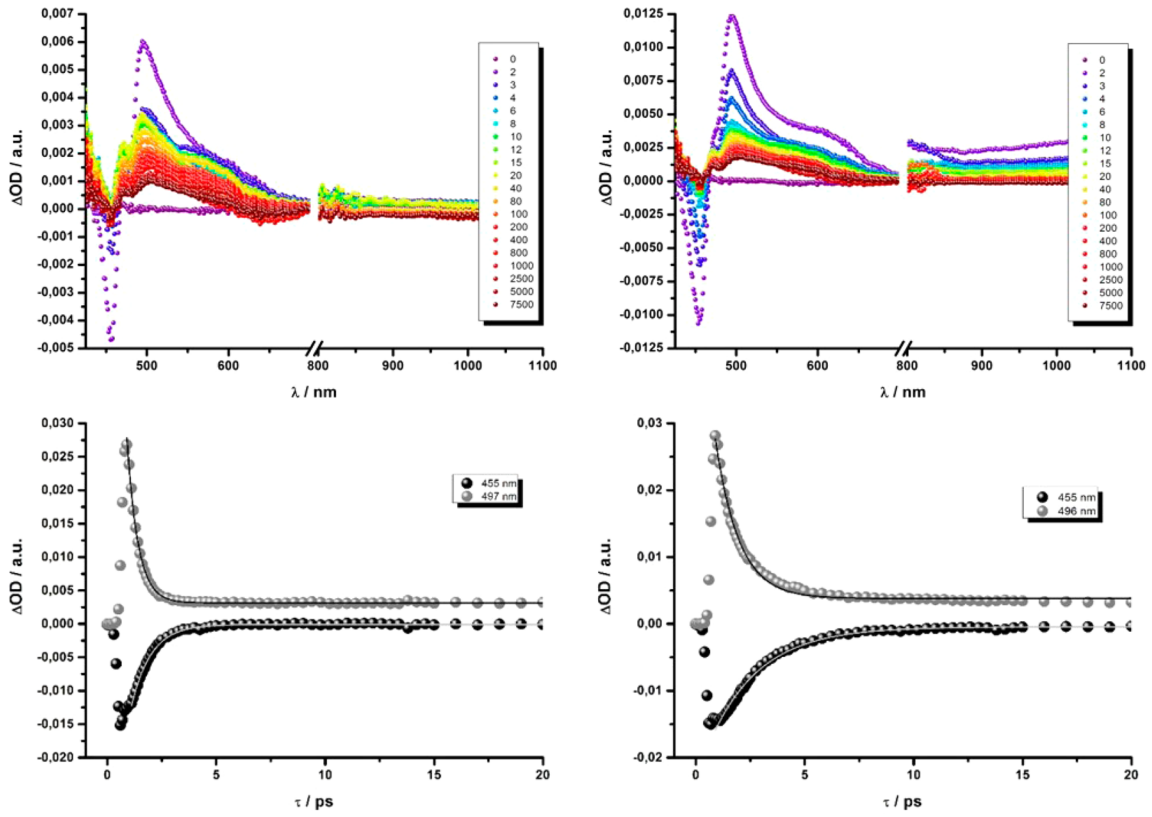

Figure 4. (Top) Differential absorption spectra (visible and near-infrared) obtained upon femtosecond flash photolysis (387 nm, 200 nJ) of nonpassivated Cu_2O NPs (left) and passivated Cu_2O NPs (right) film with several time delays between 0 and 8000 ps at rt. (Bottom, left and right) Corresponding time-absorption profiles of the spectra at 455 and 497 nm, monitoring the exciton dynamic.

dx.doi.org/10.1021/ja502221r | J. Am. Chem. Soc. 2014, 136, 7233−7236

is red-shifted to 455 nm, the maximum is split into 475 and 495 nm features, and the shoulder is blue-shifted to 590 nm. Our observations, that is, transient bleaching at 455 nm and strong excited state absorption at wavelengths beyond 479 nm, are in sound agreement with the previous studies on Cu_2O NPs, where the nature of the signals is linked to excitonic and trap states.[22]

Regarding passivated Cu_2O NPs, again the same ground state bleaching at 450 nm, maximum at 495 nm, and shoulder at 605 nm are formed with the commencement of the excitation, right part of Figure 4. A short- and long-lived decay of the transient are seen. By fitting the short-lived decay, a lifetime for the excitonic state of 1.16 ± 0.03 ps is determined, which is approximately twice as long as that seen for nonpassivated Cu_2O. As a matter of fact, lowering the number of recombination centers via ligand exchange with MPA assists in stabilizing the excitonic state and, in turn, in activating emissive excitonic states that are either copper or oxygen bound, vide infra. Nevertheless, a long-lived component, whose features resemble those recorded for nonpassivated Cu_2O, namely a 455 nm minimum, 475 and 495 nm maxima, and a 590 nm shoulder, is noted at time delays during which the short-lived component has decayed quantitatively. Its two lifetimes are in the range of hundreds of ns and about 2 μs. Owing to the fact that their relative amplitudes have decreased by a factor of 2 when compared to nonpassivated Cu_2O suggests that the two processes are linked to each other. This hypothesis is further corroborated by the fact that the emission of passivated Cu_2O NPs is significantly stronger than that noted for nonpassivated Cu_2O NPs. The reproducibility of PL increase upon MPA treatment (see Figure S5) was probed in several PL assays, which revealed on average an increase of more than 1 order of magnitude. The lifetimes as they were derived from the transient absorption measurements are summarized in Table S1. The long-lived components on the microsecond time scale originate presumably from the defect or/trap states, while, as aforementioned, the ultrafast component on the picosecond time regime is related to an excitonic state. Such an elongation of the exciton lifetimes has previously been reported for Cu_2O quantum dots and is based on a forbidden transition across the band gap at the Γ point.[22]

To further demonstrate the influence of the ligand passivation on Cu_2O NPs, we fabricated photovoltaic devices using a simple planar heterojunction structure (see Figure S8a). Prior to any MPA treatment, no appreciable photocurrents were noted. In stark contrast, devices based on surface passivated Cu_2O NPs showed a short circuit current density (J_{sc}) of 0.85 mA cm^{-2}. Details on the device fabrication and the corresponding current−voltage characteristic are given in the SI (see Figure S8b). The observed photocurrent of 0.85 mA cm^{-2} is larger than that of previously reported values for cuprous NPs used in a similar device structure.[23] Here, an important processing advantage over the previous reports is a significantly lower annealing temperature used for device fabrication (125 °C).

In conclusion, cuprite Cu_2O NPs were prepared by using the technique of flame spray synthesis. The various analytical analyses revealed no presence of undesired CuO or pure metallic Cu. Furthermore, the concept of ligand passivation was demonstrated in Cu_2O NPs by binding mercapto (−SH) groups to the different atomic sites on the surface of nanoparticles, reducing the recombination pathways for charges dissociated from various excitonic states. The strategy of ligand surface passivation was shown to be an effective way to develop semiconductor materials with significantly lower electronic trap states within the band gap, making them suitable materials for modern electronic and optoelectronic devices.

■ ASSOCIATED CONTENT

Supporting Information

Experimental details, Figures S1−S8, and Table S1. This material is available free of charge via the Internet at http://pubs.acs.org.

■ AUTHOR INFORMATION

Corresponding Author

hamed.azimi@fau.de

Notes

The authors declare no competing financial interest.

■ ACKNOWLEDGMENTS

The authors would like to acknowledge the funding of the Deutsche Forschungsgemeinschaft (DFG) through the Cluster of Excellence Engineering of Advanced Materials, BAYER Technology Services and Solar-Fabrik AG.

■ REFERENCES

(1) Rühle, S.; Anderson, A. Y.; Barad, H.; Kupfer, B.; Bouhadana, Y.; Rosh-Hodesh, E.; Zaban, A. *J. Phys. Chem. Lett.* **2012**, *3*, 3755−3764.
(2) Yuhas, B. D.; Yang, P. *J. Am. Chem. Soc.* **2009**, *131*, 3756−3761.
(3) Zhang, J.; Liu, J.; Peng, Q.; Wang, X.; Li, Y. *Chem. Mater.* **2006**, *18*, 867−871.
(4) Musa, A. O.; Akomolafe, T.; Carter, M. J. *Sol. Energy Mater. Sol. Cells* **1998**, *51*, 305−316.
(5) Poizot, P.; Laruelle, S.; Grugeon, S.; Dupont, L.; Tarascon, J. M. *Nature* **2000**, *407*, 496−499.
(6) Chaudhary, Y.; Agrawal, A.; Shrivastava, R.; Satsangi, V. R.; Dass, S. *Int. J. Hydrogen Energy* **2004**, *29*, 131−134.
(7) Miyake, M.; Chen, Y.-C.; Braun, P. V.; Wiltzius, P. *Adv. Mater.* **2009**, *21*, 3012−3015.
(8) Kalidindi, S. B.; Sanyal, U.; Jagirdar, B. R. *Phys. Chem. Chem. Phys.* **2008**, *10*, 5870−4.
(9) Graetzel, M.; Janssen, R. A. J.; Mitzi, D. B.; Sargent, E. H. *Nature* **2012**, *488*, 304−12.
(10) Tang, J.; Kemp, K. W.; Hoogland, S.; Jeong, K. S.; Liu, H.; Levina, L.; Furukawa, M.; Wang, X.; Debnath, R.; Cha, D.; Chou, K. W.; Fischer, A.; Amassian, A.; Asbury, J. B.; Sargent, E. H. *Nat. Mater.* **2011**, *10*, 765.
(11) Barkhouse, D. A. R.; Pattantyus-Abraham, A. G.; Levina, L.; Sargent, E. H. *ACS Nano* **2008**, *2*, 2356−62.
(12) Ip, A. H.; Thon, S. M.; Hoogland, S.; Voznyy, O.; Zhitomirsky, D.; Debnath, R.; Levina, L.; Rollny, L. R.; Carey, G. H.; Fischer, A.; Kemp, K. W.; Kramer, I. J.; Ning, Z.; Labelle, A. J.; Chou, K. W.; Amassian, A.; Sargent, E. H. *Nat. Nanotechnol.* **2012**, *7*, 577−82.
(13) Yin, M.; Wu, C.-K.; Lou, Y.; Burda, C.; Koberstein, J. T.; Zhu, Y.; O'Brien, S. *J. Am. Chem. Soc.* **2005**, *127*, 9506−11.
(14) Ghijsen, J.; Tjeng, L. H.; van Elp, J.; Eskes, H.; Westerink, J.; Sawatzky, G. A.; Czyzyk, M. T. *Phys. Rev. B* **1988**, *38*, 11322−11330.
(15) Robert, T.; Bartel, M.; Offergeld, G. *Surf. Sci.* **1972**, *33*, 123−130.
(16) Liu, X.-W.; Wang, F.-Y.; Zhen, F.; Huang, J.-R. *RSC Adv.* **2012**, *2*, 7647.
(17) Xu, R.; Zeng, H. C. *Langmuir* **2004**, *20*, 9780.
(18) Yao, K. X.; Yin, X. M.; Wang, T. H.; Zeng, H. C. *J. Am. Chem. Soc.* **2010**, *132*, 6131−6144.
(19) Gastev, S. V.; Kaplyanskii, A. A.; Sokolov, N. S. *Solid State Commun.* **1982**, *42*, 389−391.
(20) Solache-Carranco, H.; Juárez-Díaz, G.; Esparza-García, a.; Briseño-García, M.; Galván-Arellano, M.; Martínez-Juárez, J.; Romero-Paredes, G.; Peña-Sierra, R. *J. Lumin.* **2009**, *129*, 1483−1487.
(21) Raebiger, H.; Lany, S.; Zunger, A. *Phys. Rev. B* **2007**, *76*, 45209.
(22) Burda, C.; Lou, Y. *Electrochem. Soc. Proc.* **2004**, *22*, 274.
(23) Hung, L.-I.; Tsung, C.-K.; Huang, W.; Yang, P. *Adv. Mater.* **2010**, *22*, 1910−1914.